Geophysical Research Letters

RESEARCH LETTER
10.1029/2019GL084605

Radiative Forcing and Health Impact of Aerosols and Ozone in China as the Consequence of Clean Air Actions over 2012–2017

Ruijun Dang[1,2] and **Hong Liao**[3]

[1]State Key Laboratory of Atmospheric Boundary Layer Physics and Atmospheric Chemistry (LAPC), Institute of Atmospheric Physics, Chinese Academy of Sciences, Beijing, China, [2]University of Chinese Academy of Sciences, Beijing, China, [3]Collaborative Innovation Center of Atmospheric Environment and Equipment Technology/Joint International Research Laboratory of Climate and Environment Change, School of Environmental Science and Engineering, Nanjing University of Information Science and Technology, Nanjing, China

Key Points:
- Concentrations of $PM_{2.5}$ decreased, and those of O_3 increased as a result of air pollution control over 2012–2017
- Changes in $PM_{2.5}$ and O_3 led to a positive radiative forcing of 1.26 W/m^2 over eastern China (20–45°N, 105–122.5°E)
- Changes in air pollution exposures are estimated to avoid 268.3 thousand deaths in eastern China

Supporting Information:
- Supporting Information S1

Correspondence to:
H. Liao,
hongliao@nuist.edu.cn

Citation:
Dang, R., & Liao, H. (2019). Radiative forcing and health impact of aerosols and ozone in China as the consequence of clean air actions over 2012–2017. *Geophysical Research Letters*, *46*, 12,511–12,519. https://doi.org/10.1029/2019GL084605

Received 18 JUL 2019
Accepted 5 OCT 2019
Published online 5 NOV 2019

Abstract We applied the chemical transport model GEOS-Chem to examine the changes in aerosols and tropospheric O_3 in China from 2012–2017 and the associated radiative forcing and health impact. Simulated surface layer concentrations and column burdens of aerosols and O_3 were evaluated by comparing with ground-based and satellite-retrieved measurements. Between 2012 and 2017, simulated annual mean concentrations of $PM_{2.5}$ decreased by 21.0%, while O_3 increased by 11.9% over eastern China (20–45°N, 105–122.5°E). Changes in aerosols and O_3 over 2012–2017 jointly exerted a positive radiative forcing of 1.26 W/m^2 over eastern China, which was dominated by the less cooling from $PM_{2.5}$ reductions (1.18 W/m^2). The Global Exposure Mortality Model predicted 268.3 (247.3–291.6) thousand (9.6%) fewer deaths in eastern China in 2017 relative to 2012. These results suggest an appreciable health benefit and a potential warming as a consequence of clean air actions.

Plain Language Summary Stringent clean air actions have been implemented in China since 2013, aiming to improve air quality. As a result, observed concentrations of aerosols decreased while those of O_3 increased in eastern China. In this work we assess the radiative forcing and health impact resulted from the changes in aerosols and O_3 in China for the period of 2012–2017 by using a chemical transport model. The model reproduces the observed changes in $PM_{2.5}$ and O_3 in recent years and estimates a net positive radiative forcing of 1.26 W/m^2 in 2017 relative to 2012 over eastern China. Further estimates from the mortality model show that approximately 270,000 deaths are avoided. Results from our study suggest an appreciable health benefit as well as a potential warming as a consequence of clean air actions over 2012–2017.

1. Introduction

Air pollution has been a serious issue in China and has drawn the intense concern of the government. Starting in 2013, stringent clean air actions were taken in China, aiming to significantly improve air quality by 2017 (*Action Plan on Air Pollution Prevention and Control*, 2013). Consequently, Chinese anthropogenic emissions of SO_2, NO_x, CO, BC, and OC decreased by 21–59% from 2013 to 2017 (Zheng et al., 2018), and the average $PM_{2.5}$ concentrations in 74 cities across China fell by 33.3% (16.3% to 50.3%; Huang et al., 2018). Meanwhile, O_3 pollution has not improved and is seemingly getting worse (Huang et al., 2018; *K*. Li et al., 2019; *X*. Lu et al., 2018; Ma et al., 2016; Sun et al., 2016). Observed annual mean O_3 concentrations during 2013–2017 were reported to change by 20.4% (−30.1% to 71.0%) in 74 key cities in China (Huang et al., 2018), and the summertime maximum daily average 8-hr (MDA8) O_3 levels averaged over these cities increased by approximately 20% when concentrations in 2016–2017 were compared to those in 2013–2014 (*X*. Lu et al., 2018). Since $PM_{2.5}$ and O_3 changed so drastically and differently over the period of 2012–2017, estimates of the associated net radiative forcing and health impact are important for reexamining the clean air actions and for future planning.

Exposure to $PM_{2.5}$ and O_3 was estimated to cause 4.2 million and 254,000 deaths worldwide in 2015, respectively, and was reported to be a leading contributor to the global disease burden (Cohen et al., 2017). Several studies estimated the health benefits from $PM_{2.5}$ reductions alone in China in recent years (Bi et al., 2019; *X*.

©2019. American Geophysical Union. All Rights Reserved.

C. Lu et al., 2019). By using satellite-retrieved $PM_{2.5}$ data, *X. C*. Lu et al. (2019) reported a decrease in annual premature mortalities from 1.1 million in 2014 to 0.96 million in 2017 for China. However, few studies have assessed the net health effect from changes in both $PM_{2.5}$ and O_3 in recent years. Based on ground-based observations during 2013–2017, Huang et al. (2018) found that although O_3-attributed deaths showed an increase of 7.7 thousand, the overall premature mortality figure decreased by a total of 47.2 thousand in 74 key cities across China. A more comprehensive estimation is therefore needed to have full coverage of China.

Both aerosols and tropospheric O_3 play important roles in regional/global climate as short-lived forcers. Aerosols influence climate directly through scattering and absorbing infrared and solar radiation, and indirectly by altering cloud properties. Since preindustrial times, aerosols are estimated to have a global mean radiative forcing of −0.9 (−1.5 to −0.4) W/m^2 (including both aerosol-radiation and aerosol-cloud interactions), partially mitigated the positive radiative forcing of 2.83 (2.26 to 3.40) W/m^2 by long-lived greenhouse gases (*IPCC*, 2013). Tropospheric O_3 is a greenhouse gas with anthropogenic radiative forcing of 0.40 (0.2 to 0.6) W/m^2 (*IPCC*, 2013). Variations in ozone concentrations contribute to the climate change in the Northern and Southern Hemispheres and even influence precipitation in China (Son et al., 2009; Xie et al., 2016; Xie et al., 2017; Xie et al., 2018). Given these factors, efforts to improve air quality always come with climate consequences, as demonstrated by developed countries in North America and Europe over the past decades. Leibensperger et al. (2012a) reconstructed the historical aerosol trends in the United States and simulated a positive direct radiative forcing (DRF) of 0.8 W/m^2 and a positive indirect radiative forcing of 1.0 W/m^2 over the eastern United States between 1980 and 2010 when strict emission reduction regulations were enforced. As a result, a strong regional warming of 0.35 °C was identified in the eastern United States between 1980 and 2010 by the transient climate simulations with Goddard Institute for Space Studies general circulation model 3 (Leibensperger et al., 2012b). Similarly, in Europe during its air quality control period, the decrease in aerosols led to a positive European mean radiative forcing (direct plus indirect) of 1.26 W/m^2 between 1981–1985 and 2001–2005, while the increase in O_3 also exerted a positive radiative forcing with a smaller magnitude of 0.05 W/m^2 (Pozzoli et al., 2011). In this regard, the radiative forcing resulted from the changes in air quality in China in recent years is of particular interest because of the very high concentrations of aerosols and O_3 in China and the increasingly stringent air quality control policies.

In this study, we use the global 3-D chemical transport model GEOS-Chem to simulate the changes in $PM_{2.5}$ and tropospheric O_3 over China from 2012 to 2017. Associated changes in radiative forcing are calculated by the coupled radiative transfer module Rapid Radiative Transfer Model (RRTMG), while attributable mortalities are estimated based on health impact functions with simulated $PM_{2.5}$ and O_3 concentrations as the inputs. Integrated or respective roles of $PM_{2.5}$ and O_3 are all examined.

2. Methods

We simulate concentrations of aerosols and O_3 using the nested grid version (0.5° latitude by 0.625° longitude over Asia 11°S to 55°N, 60–150°E) of the GEOS-Chem model (version 11-01; http://acmg.seas.harvard.edu/geos/) driven by Modern-Era Retrospective Analysis for Research and Applications Version (MERRA-2) assimilated meteorological data (Gelaro et al., 2017). The model includes fully coupled O_3-NO_x-hydrocarbon chemistry (Bey et al., 2001; Park et al., 2004) and online aerosol calculations including sulfate (Park et al., 2004), nitrate (Pye et al., 2009), ammonium, black carbon and organic carbon (Park et al., 2003), mineral dust (Fairlie et al., 2007), and sea salt (Alexander et al., 2005). Photolysis rates are computed by Fast-JX scheme (Bian & Prather, 2002). Stratospheric O_3 is simulated based on linearized O_3 parameterization (LINOZ; McLinden et al., 2000). Aerosol thermodynamic equilibrium is calculated by the ISORROPIA II package (Fountoukis & Nenes, 2007). Heterogeneous reactions of aerosols, such as irreversible absorption of NO_3 and NO_2 on wet aerosols (Jacob, 2000), hydrolysis of N_2O_5 (Evans & Jacob, 2005), and the uptake of HO_2 by aerosols (Thornton et al., 2008) are included. Dry deposition for gas and aerosols is computed based on the resistance-in-series model (*Y. H*. Wang et al., 1998; Wesely, 1989), and wet deposition follows the scheme of Liu et al. (2001). $PM_{2.5}$ concentration is calculated as the sum of sulfate, nitrate, ammonium, BC, and OC from the model; sea salt and mineral dust aerosols are not considered in $PM_{2.5}$ in this study because they are emitted naturally.

Global anthropogenic emissions in the GEOS-Chem model are from the Community Emissions Data System (Hoesly et al., 2018). For emissions in China, the emissions from Shared Socioeconomic Pathways (Gidden et al., 2019) for year 2015 are used and the annual scaling factors from Zheng et al. (2018) are applied to obtain emissions for other years during 2012–2017. Biomass burning emissions follow the Global Fire Emissions Database Version 4 (van der Werf et al., 2017), and biogenic volatile organic compounds emissions are calculated online by Model of Emissions of Gases and Aerosols from Nature Version 2 (Guenther et al., 2006). Other natural emissions such as NO_x from lighting and soil are computed based on MERRA-2 meteorology. From 2012 to 2017, annual emissions (anthropogenic plus natural) of SO_2, OC, BC, CO, and NO_x decreased sharply over eastern China (105–122.5°E, 20–45°N) by 62.1%, 29.4%, 28.9%, 22.0%, and 21.1%, respectively (Figure S1 in the supporting information), and the largest reductions centered in densely populated city clusters including the North China Plain, the Yangtze River Delta, the Pearl River Delta, Fenwei Plain, central China (e.g., Hubei and Hunan provinces) and the Sichuan Basin (Figure S2). Emissions of NH_3 experienced a small decrease of 4.6%, while nonmethane volatile organic compounds emissions increased by 3.3%.

The all-sky DRF of each aerosol species and O_3 is calculated via the online coupled radiative transfer module RRTMG (for general circulation models). The RRTMG resolves the spectrum to 14 shortwave bands and 16 longwave bands covering wavelengths from 0.23 to 56 μm. Microphysical properties of each species follow Heald et al. (2014). Instantaneous shortwave and longwave radiative fluxes are computed every 3 hr. The DRF of each species is calculated as the difference of parallel simulations with and without anthropogenic emissions.

The baseline simulations include changes in both emissions and meteorology from 2012 to 2017, and there is a 6-month spin-up before January 2012. Associated premature mortalities are estimated based on simulated concentrations and the specific steps are described in section 3.4.

3. Results and Discussions

3.1. Model Evaluation

Here we conduct comparisons with ground-based and satellite-retrieved measurements (described in Text S1) to see whether the nested grid version of the GEOS-Chem model with the emissions described in section 2 can reproduce the magnitudes and spatiotemporal patterns of surface layer $PM_{2.5}$ and O_3 concentrations, aerosol optical depth (AOD), and tropospheric column ozone (TCO).

Simulated surface layer $PM_{2.5}$ and O_3 concentrations are evaluated using measurements from the CNEMC data set over the period of 2014–2017. Nationwide 841 sites are selected from the CNEMC data set and averaged on the MERRA-2 grid (corresponding to 243 model grids) for comparison. Figure S3 displays the spatial distributions of simulated and observed seasonal mean $PM_{2.5}$ concentrations in four seasons for 2014–2017. The model reproduces the observed spatial distributions of seasonal mean $PM_{2.5}$, with high correlation coefficients (r) ranging from 0.75 to 0.83 and normalized mean biases (NMB) of 2.0–34.1% for different seasons. In June–August (JJA), March–May, and September–November (SON), both simulated and observed seasonal mean $PM_{2.5}$ levels were highest over the North China Plain. In DJF, severely polluted zones extended to a larger area of China (including eastern China, northeastern China, and the Sichuan Basin) as shown by a number of grids with both observed and simulated $PM_{2.5}$ exceeding 100 $\mu g/m^3$. The model also reproduces the features of $PM_{2.5}$ seasonality, with a high r value of 0.79 between observed and simulated monthly mean $PM_{2.5}$ for the ensemble of 243 grids (Figure S4). The monthly mean $PM_{2.5}$ from both simulations and observations peaks in wintertime due to the strengthened anthropogenic emissions as well as low temperatures favoring nitrate ammonium formation and shows valleys during summertime because of the enhanced wet removal from the East Asian summer monsoon.

Regarding surface O_3, the model generally captures the observed seasonal mean spatial patterns in DJF, JJA and SON with r values of 0.60, 0.30, and 0.41, respectively (Figure S5). Observed O_3 hot spots such as the Pearl River Delta in DJF, northern China in JJA, and the coastal areas (including Shandong province, the Yangtze River Delta, and the Pearl River Delta) in SON are well reproduced by the model. In March–May, compared with measurements, the model has low biases over the North China Plain and the Yangtze River Delta (with a NMB of −25.7%), whereas high biases outside these two regions (with a NMB

of +29.3%), which lead to a low coefficient correlation over the whole of China when taking all grids into account. Over four seasons, the model generally overestimates O_3 concentrations with NMBs in the range of 1.0–35.8%. Monthly variations of surface layer O_3 are also captured by the model with a high r value of 0.65 between observed and simulated monthly mean O_3 concentrations for the ensemble of 243 grids (Figure S4). Both simulated and observed monthly mean O_3 concentrations are high during warm months (April to September), which are driven by enhanced photochemical O_3 production owing to high temperatures and strengthened natural emissions of O_3 precursors.

Estimation of radiative forcing of air pollutants relies not only on surface layer concentrations but also on column burdens. Simulated AOD and TCO are thus compared with the satellite retrievals from Moderate Resolution Imaging Spectroradiometer (MODIS) and Ozone Monitoring Instrument/Microwave Limb Sounder (OMI/MLS), respectively (Figures S6 and S7). For 2012–2017, observed annual mean MODIS AOD exhibited high values of 0.8–1.0 over eastern China with hot spots occurring in the North China Plain, the Yangtze River Delta, the Sichuan Basin, and central China. This spatial distribution of AOD is well captured by the model with low biases over the Yangtze River Delta and Xinjiang province and high biases over the Sichuan Basin and Northeast China. Simulated AOD averaged over China is 0.30, very close to the value from MODIS observation (0.27). Good agreement is also found between the simulated and observed TCO. Both simulated and OMI/MLS retrieved annual mean TCO show high values of 35–45 DU over eastern China and low values of 20–30 DU over the Tibet plateau. For 2012–2017, simulated annual mean TCO is 33.3 DU over whole China, a little smaller than the value of 35.5 DU from the OMI/MLS data set.

We also examine the changes in annual mean surface layer concentrations of $PM_{2.5}$ and O_3, AOD, and TCO in China, to see whether the model can capture the observed changes in recent years. From 2014 to 2017 when CNEMC data are available, observed annual mean $PM_{2.5}$ averaged over the 243 grids decreased rapidly by 15.6 $\mu g/m^3$ in 2017 relative to 2014, and observed annual mean O_3 increased by 4.6 ppbv in 2017 (Figure S8a). The model satisfactorily captures these tendencies of changes but with smaller magnitudes; between 2014 and 2017, simulated $PM_{2.5}$ and O_3 show changes of −10.6 $\mu g/m^3$ and 3.1 ppbv, respectively, when simulated values are averaged over the 243 grids. Following the trend of the surface layer $PM_{2.5}$ concentrations, MODIS AOD decreased by 0.07 over China from 2012–2017 (Figure S8b). The model reproduces the decrease in AOD, with a simulated decrease of 0.07 over China. While the observed surface layer O_3 increased, TCO from OMI/MLS shows a decrease of 1.02 DU over 2012–2017 for China, which may be attributed to the relatively high bias in its 2012 levels (according to Figures S7 and Figure 8a in a previous work; Ziemke et al., 2019). Despite this, the model captures the interannual variation of TCO and simulates an increase of 1.81 DU over 2012–2017. Overall, the baseline simulation can reproduce the surface layer concentrations and column burdens of aerosols and tropospheric O_3 in China reasonably well.

3.2. Simulated Changes in Air Quality in China From 2012 to 2017

Figure 1 shows the simulated changes in annual mean surface layer $PM_{2.5}$, AOD, surface layer O_3, and TCO over China from 2012 to 2017. Simulated $PM_{2.5}$ concentrations were highest over eastern China, with a regional mean value of 50.0 $\mu g/m^3$ in 2012 before the start of clean air actions. From then on, $PM_{2.5}$ levels began to drop rapidly and by 2017 had decreased 10.5 $\mu g/m^3$ (21.0%) over eastern China, with largest changes (−16 to −40 $\mu g/m^3$) found in the North China Plain, the Sichuan Basin, and central China. Simulated AOD shows a similar spatiotemporal pattern as the simulated $PM_{2.5}$. The AOD over eastern China decreased from 0.52 in 2012 to 0.39 in 2017 with a relative change of −25.0%.

Simulated annual mean surface layer O_3 levels are highest over western China (>55 ppbv) because of the large downward transport from the stratosphere. Over eastern China, simulated surface-layer O_3 had a mean value of 37.23 ppbv in eastern China in 2012 and increased gradually thereafter by 4.44 ppbv (11.9%) in 2017. The largest increases of O_3 of 5–10 ppbv were simulated in eastern China (including the North China Plain and the Yangtze River Delta). Such increases in O_3 concentration can be partly attributed to the contemporaneous $PM_{2.5}$ reductions according to K. Li et al. (2019), because the decrease of $PM_{2.5}$ can lead to a slowdown of the aerosol sink of HO_2 radicals and thus accelerate the O_3 production. Following the tendency of changes in surface O_3, simulated TCO over eastern China increased by 2.95 DU (7.8%) over 2012–2017.

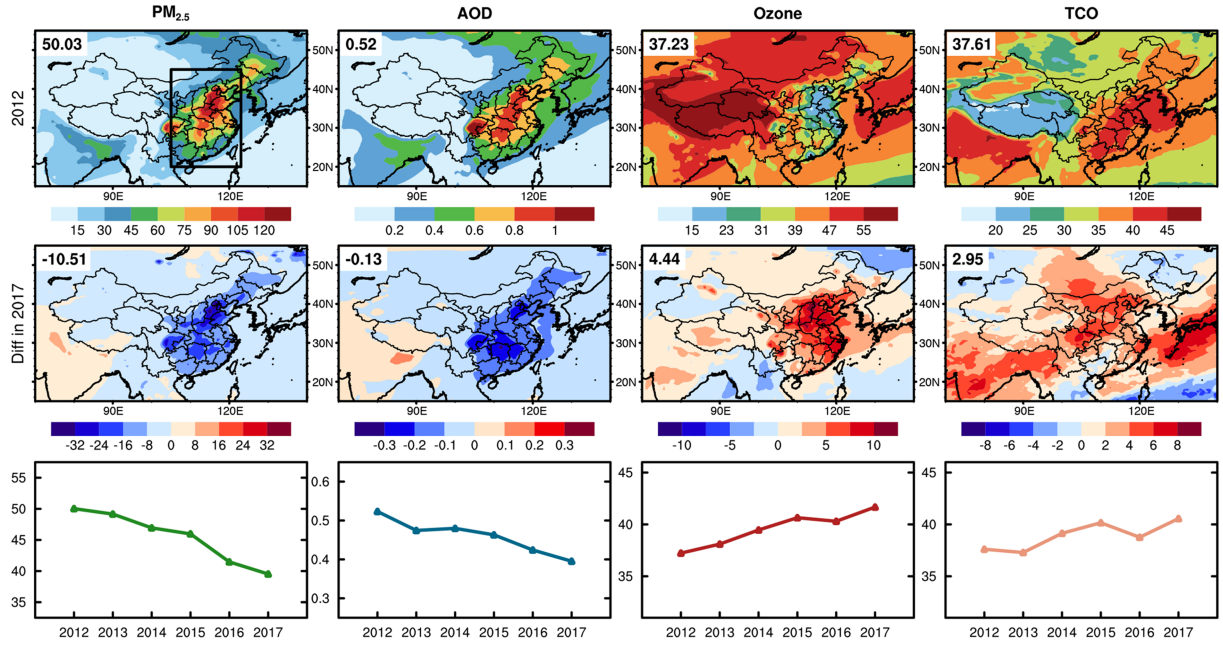

Figure 1. Simulated spatial distributions and temporal evolutions of surface $PM_{2.5}$ ($\mu g/m^3$), AOD, surface O_3 (ppbv), and TCO (DU). The top row shows the spatial distributions in 2012; the middle row shows the changes between 2012 and 2017 (values in 2017 minus those in 2012); and the bottom row shows the temporal evolutions from 2012–2017 for eastern China (105–122.5°E, 20–45°N). The averaged value over eastern China (marked by the black rectangle in the first panel) is indicated at the top left corner of each panel of the top and the middle rows. AOD = aerosol optical depth; TCO = tropospheric column ozone.

3.3. Radiative Forcing From Aerosols and Tropospheric O_3 in China Over 2012–2017

The all-sky DRF at the tropopause by aerosols and tropospheric O_3 is presented in Figure 2. In 2012, aerosol DRF was the strongest (−10 to −16 W/m^2) over the North China Plain, the Sichuan Basin and central China, which is consistent with the spatial distribution of AOD in 2012 (Figure 1). The aerosol DRF averaged over eastern China was −7.80 W/m^2 in 2012, which was slightly larger than the values (−4.8 to −6.08 W/m^2) estimated by previous studies (Chang et al., 2009; *J. W.* Li et al., 2013; *K.* Li et al., 2016; Qian et al.,

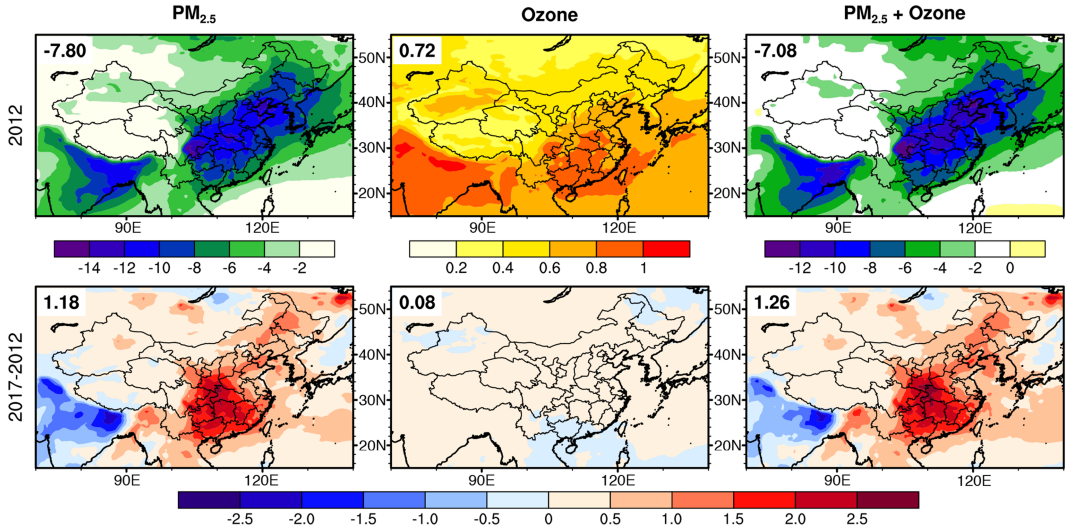

Figure 2. Simulated spatial distributions of annual mean all-sky direct radiative forcing (W/m^2) of aerosols, O_3, and aerosols plus O_3 at the tropopause in 2012 (top row) and in 2017 relative to 2012 (bottom row). Mean value for eastern China is indicated at the top left corner of each panel.

2003) as listed in Table S1. These differences in estimated aerosol DRF can be caused by discrepancies in anthropogenic emissions, chemical mechanisms of the models as well as the treatment of aerosol optical properties. In 2017 as compared to 2012, a strong positive aerosol DRF of about 2.0 W/m^2 is found at the tropopause covering the Sichuan Basin, central China, and Guizhou-Guangxi provinces (Figure 2), which is consistent with the spatial distribution of the changes in AOD between 2012 and 2017 (Figure 1). The aerosols are estimated to have a positive DRF of 1.18 W/m^2 over eastern China in 2017 relative to 2012, which is mostly contributed by the less cooling of 1.55 W/m^2 from sulfate aerosols (Figure S9). The decrease in absorbing aerosol BC exerts a cooling of −0.44 W/m^2 over eastern China, partly counteracts the warming effect resulted from the reductions in scattering aerosols (Figure S9).

Simulated all-sky tropopause DRF of tropospheric O_3 is found to be highest over eastern China (0.6–1.0 W/m^2) in 2012, resembling the spatial distribution of TCO (Figure 1). The averaged DRF of tropospheric O_3 is 0.72 W/m^2 over eastern China in 2012, comparable to the values (0.53 to 0.87 W/m^2) obtained by other studies (Chang & Liao, 2009; Chang et al., 2009; *W*. Wang et al., 2005; Zhu & Liao, 2016) in Table S1. From 2012 to 2017, the increase in tropospheric O_3 enhanced the warming, with a positive DRF of 0.08 W/m^2 over eastern China (Figure 2). Over the studied period of 2012–2017, the positive DRF caused by O_3 increases is much smaller than the positive DRF brought by reductions in aerosols.

When considering effects of both aerosols and tropospheric O_3, the net DRF from the changes in aerosols plus tropospheric O_3 during 2012–2017 is 1.26 W/m^2 at the tropopause over eastern China, which is spatially dominated by the pattern of changes in aerosols. Figure S10 also shows the DRF at the surface. Over the 2012–2017 period, changes in aerosols and O_3 are estimated to exert a positive surface DRF of 3.66 and 0.08 W/m^2, respectively, for eastern China. The *IPCC* (2013) has reported a global warming of 0.85 °C (0.65–1.06 °C) in surface temperature between 1880 and 2012, and the related global mean radiative forcing values of well-mixed greenhouse gases, tropospheric O_3, and aerosols are +2.83, +0.4, and −0.9 W/m^2, respectively, in 2011 compared to 1,750 levels. Therefore, our predicted net DRF (aerosols plus tropospheric O_3) of 1.26 W/m^2 over eastern China in 2017 relative to 2012 is very large and has important implications for regional climate.

3.4. Health Impacts of $PM_{2.5}$ and O_3 in China From 2012 to 2017

The premature mortalities attributable to the ambient air pollutants exposures are calculated following the approach from Apte et al. (2015), which can be briefly described as

$$\Delta \boldsymbol{Mortality} = \boldsymbol{y_0}\left(\frac{\boldsymbol{RR}(\boldsymbol{C})-\boldsymbol{1}}{\boldsymbol{RR}(\boldsymbol{C})}\right)\boldsymbol{Pop} \quad (1)$$

where $\Delta\boldsymbol{Mortality}$ is the premature mortality caused by $PM_{2.5}$ or O_3 exposures, $\boldsymbol{y_0}$ is the baseline mortality rate for a specific disease, $\boldsymbol{Pop}$ is the exposed population, and $\boldsymbol{RR}(\boldsymbol{C})$, referred as concentration-response functions (CRFs), relate changes in air pollutant concentrations $\boldsymbol{C}$ to changes in relative risk $\boldsymbol{RR}$ for each specific disease (see Text S2 for details). For O_3, we use the CRF from Jerrett et al. (2009) that associates long-term O_3 exposures to the relative risk of respiratory diseases. For $PM_{2.5}$, two kinds of CRFs are applied for further comparisons. One is the integrated exposure-response model (IER) from *R. T*. Burnett et al. (2014), which is widely used in the mortality estimations in the global burden of disease, World Health Organization, and many previous studies (Apte et al., 2015; Huang et al., 2018; *X. C*. Lu et al., 2019). The IER is a disease-specific model that is constructed for five causes of deaths by $PM_{2.5}$ including lower respiratory infections (LRI), chronic obstructive pulmonary disease, lung cancer, ischemic heart disease, and stroke. Another CRF we used is the recent Global Exposure Mortality Model (GEMM), which relaxed several strong assumptions required by IER and is assumed to provide better estimates for highly polluted environments such as China (*R*. Burnett et al., 2018). The GEMM comprises two forms of applications, which are GEMM 5-COD and GEMM noncommunicable disease (NCD) + LRI; the first one is used for estimating separate mortality by five causes of deaths aforementioned (5-COD: LRI, chronic obstructive pulmonary disease, LC, ischemic heart disease, and stroke), thus fitting for the comparison with assessments from the IER; and the second one aims for broader causes of deaths as the sum of NCDs and LRI.

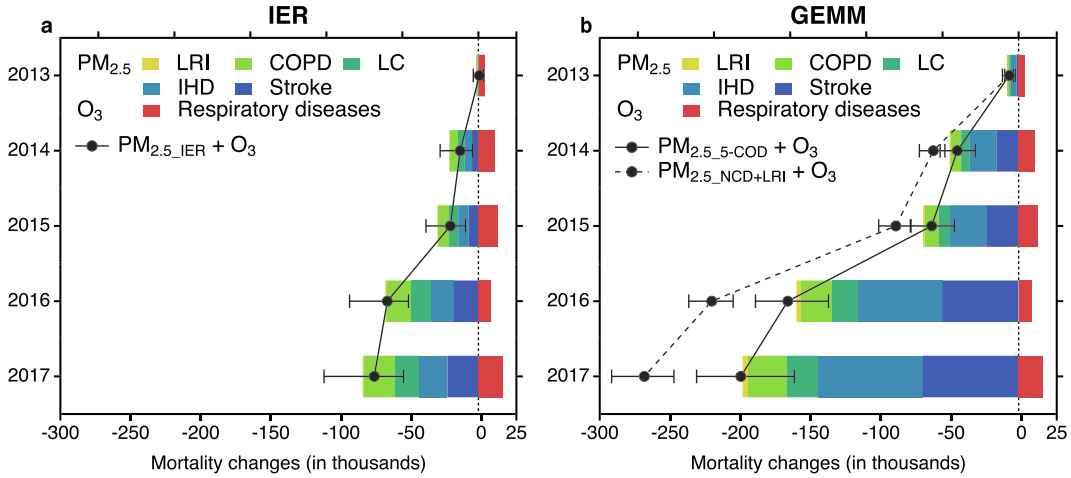

Figure 3. Annual deaths (in thousands) caused by ambient $PM_{2.5}$ and O_3 exposures in eastern China from 2013 to 2017 relative to 2012 levels. For $PM_{2.5}$, estimates based on two different models (a) IER and (b) GEMM are displayed. Bars indicate the estimates for each specific cause of death attributable to $PM_{2.5}$ and O_3. Black lines indicate the total estimates of $PM_{2.5}$ plus O_3. Error bars indicate the 95% confidence interval (CI). In (b), total estimates from GEMM noncommunicable disease + LRI are indicated in the dashed line. IER = integrated exposure-response model; GEMM = Global Exposure Mortality Model; LRI = lower respiratory infections; IHD = ischemic heart disease; COPD = chronic obstructive pulmonary disease; LC = lung cancer.

Figure 3 shows the estimated annual deaths owing to ambient O_3 and $PM_{2.5}$ (based on two CRFs) pollutions in eastern China from 2013 to 2017 relative to 2012 levels. The increases in O_3 concentrations resulted in more deaths of respiratory diseases over the period, with increased numbers varied from 4.4 thousand in 2013 to 16.0 thousand in 2017 for eastern China. As for $PM_{2.5}$, the attributable deaths show a continuous decline. By 2017, the improvement of $PM_{2.5}$ pollution is estimated to led to 84.5, 198.3, and 284.3 thousand avoided deaths in eastern China based on IER, GEMM 5-COD, and GEMM NCD + LRI, respectively, far offsetting the excess deaths brought by O_3 increase. The estimates from GEMM are much larger than those from IER (a ratio of 0.3–0.4 between IER and GEMM), suggesting that more health benefits may come along with the improvement of $PM_{2.5}$ pollution than what previous studies have expected. Overall, changes in $PM_{2.5}$ and O_3 are estimated to ease the burden of disease from ambient air pollution in eastern China by −5.9%, −8.4%, and −9.6% with avoided deaths numbers of 68.55 (95% CI: 49.3–101.6) thousand, 182.35 (95% CI: 147.3–211.4) thousand and 268.32 (95% CI: 247.3–291.6) thousand based on IER, GEMM 5-COD, and GEMM NCD + LRI, respectively. For more information on estimates for full coverage of China, please see Table S2.

4. Conclusions

We calculate the radiative forcing and premature mortality from aerosols and O_3 in China for the air pollution control period of 2012–2017 by using the GEOS-Chem model. Simulated surface-layer concentrations and column burdens of aerosols and O_3 are evaluated using the ground-based and satellite-retrieved measurements. Between 2014 and 2017, the model satisfactorily reproduces the observed 71.3% decrease in surface layer $PM_{2.5}$ concentration and 72.1% increase in surface layer O_3 concentration averaged over 243 grids across China.

Over the 2012–2017 period, simulated annual mean concentration of $PM_{2.5}$ decreased by 21.0% over eastern China (105–122.5°E, 20–45°N) and that of O_3 increased by 11.9%. Reductions in aerosols led to a warming effect on the Earth system with a regional mean tropopause DRF of 1.18 W/m^2 over eastern China in 2017 relative to 2012. The increase in tropospheric O_3 also resulted in a positive DRF, with a smaller magnitude of 0.08 W/m^2 over eastern China. Further mortality assessment shows that $PM_{2.5}$ reductions avoided 284.3 thousand deaths in eastern China in 2017 relative to 2012 based on GEMM NCD + LRI, far offsetting the excess deaths (16.0 thousand) caused by O_3 increases. In summary, changes in $PM_{2.5}$ and O_3 from 2012–2017 are estimated to jointly exerted a positive DRF of 1.26 W/m^2 and led to 268.3 (95% CI: 247.3–291.6) thousand (9.6%) fewer deaths in eastern China.

The results in our study show an appreciable health benefit related to air pollution control from 2012 to 2017 in China, indicating a great effectiveness of clean air actions in terms of health impact. However, a potentially warming effect is also suggested on regional climate, which should be considered in future planning. It should be noted that the GEOS-Chem model is driven by assimilated meteorological fields MERRA-2, and the feedbacks between meteorology and air pollutants are not included. Fully coupled chemistry-climate model estimates are thus needed to better understand the climatic responses to the control of anthropogenic emissions.

Acknowledgments
This work was supported by the National Natural Science Foundation of China under Grants 91544219, 91744311, and 41475137. All data used in this study can be accessed publicly. Network observations of PM2.5 and O3 concentrations are obtained from the China National Environmental Monitoring Center (http://106.37.208.233:20035/); satellite AOD product is available at https://giovanni.gsfc.nasa.gov/giovanni/ website; OMI/MLS TCO product is downloaded from https://acd-ext.gsfc.nasa.gov/Data_services/cloud_slice/new_data.html website; the baseline mortality rates of diseases are obtained from Global Health Estimates by World Health Organization (https://www.who.int/healthinfo/global_burden_disease/estimates/en/); the gridded population is downloaded from the website http://sedac.ciesin.columbia.edu/data/collection/gpw-v4 and the percentage of population by age groups is from the United Nations estimates (https://population.un.org/wpp/Download/Standard/Population/). The model output used in this study can be accessed via doi (https://doi.org/10.7910/DVN/FMU2TN). We acknowledge the efforts of the GEOS-Chem working groups for developing and managing the model.

References

Alexander, B., Park, R. J., Jacob, D. J., Li, Q. B., Yantosca, R. M., Savarino, J., et al. (2005). Sulfate formation in sea-salt aerosols: Constraints from oxygen isotopes. *Journal of Geophysical Research-Atmospheres*, *110*(D10), 12. https://doi.org/10.1029/2004jd005659

Apte, J. S., Marshall, J. D., Cohen, A. J., & Brauer, M. (2015). Addressing global mortality from ambient PM2.5. *Environmental Science & Technology*, *49*(13), 8057–8066. https://doi.org/10.1021/acs.est.5b01236

Bey, I., Jacob, D. J., Yantosca, R. M., Logan, J. A., Field, B. D., Fiore, A. M., et al. (2001). Global modeling of tropospheric chemistry with assimilated meteorology: Model description and evaluation. *Journal of Geophysical Research-Atmospheres*, *106*(D19), 23073–23095. https://doi.org/10.1029/2001jd000807

Bi, W. K., Chen, K., Xiao, Z. M., Tang, M., Zheng, N. Y., Yang, N., et al. (2019). Health benefit assessment of China's National Action Plan on air pollution in the Beijing-Tianjin-Hebei area. *Aerosol and Air Quality Research*, *19*(2), 383–389. https://doi.org/10.4209/aaqr.2018.08.0297

Bian, H. S., & Prather, M. J. (2002). Fast-J2: Accurate simulation of stratospheric photolysis in global chemical models. *Journal of Atmospheric Chemistry*, *41*(3), 281–296. https://doi.org/10.1023/a:1014980619462

Burnett, R., Chen, H., Szyszkowicz, M., Fann, N., Hubbell, B., Pope, C. A., et al. (2018). Global estimates of mortality associated with long-term exposure to outdoor fine particulate matter. *Proceedings of the National Academy of Sciences of the United States of America*, *115*(38), 9592–9597. https://doi.org/10.1073/pnas.1803222115

Burnett, R. T., Pope, C. A., Ezzati, M., Olives, C., Lim, S. S., Mehta, S., et al. (2014). An integrated risk function for estimating the global burden of disease attributable to ambient fine particulate matter exposure. *Environmental Health Perspectives*, *122*(4), 397–403. https://doi.org/10.1289/ehp.1307049

Chang, W. Y., & Liao, H. (2009). Anthropogenic direct radiative forcing of tropospheric ozone and aerosols from 1850 to 2000 estimated with IPCC AR5 emissions inventories. *Atmospheric and Oceanic Science Letters*, *2*(4), 201–207.

Chang, W. Y., Liao, H., & Wang, H. J. (2009). Climate responses to direct radiative forcing of anthropogenic aerosols, tropospheric ozone, and long-lived greenhouse gases in eastern China over 1951–2000. *Advances in Atmospheric Sciences*, *26*(4), 748–762. https://doi.org/10.1007/s00376-009-9032-4

Cohen, A. J., Brauer, M., Burnett, R., Anderson, H. R., Frostad, J., Estep, K., et al. (2017). Estimates and 25-year trends of the global burden of disease attributable to ambient air pollution: An analysis of data from the Global Burden of Diseases Study 2015. *Lancet*, *389*(10082), 1907–1918. https://doi.org/10.1016/s0140-6736(17)30505-6

Evans, M. J., & Jacob, D. J. (2005). Impact of new laboratory studies of N_2O_5 hydrolysis on global model budgets of tropospheric nitrogen oxides, ozone, and OH. *Geophysical Research Letters*, *32*, L09813. https://doi.org/10.1029/2005gl022469

Fairlie, T. D., Jacob, D. J., & Park, R. J. (2007). The impact of transpacific transport of mineral dust in the United States. *Atmospheric Environment*, *41*(6), 1251–1266. https://doi.org/10.1016/j.atmosenv.2006.09.048

Fountoukis, C., & Nenes, A. (2007). ISORROPIA II: A computationally efficient thermodynamic equilibrium model for K + -Ca2 + -Mg2 + -Nh(4)(+)-Na + -SO^4_2--NO_3--Cl--H_2O aerosols. *Atmospheric Chemistry and Physics*, *7*(17), 4639–4659. https://doi.org/10.5194/acp-7-4639-2007

Gelaro, R., McCarty, W., Suarez, M. J., Todling, R., Molod, A., Takacs, L., et al. (2017). The Modern-Era Retrospective Analysis for Research and Applications, Version 2 (MERRA-2). *Journal of Climate*, *30*(14), 5419–5454. https://doi.org/10.1175/jcli-d-16-0758.1

Gidden, M. J., Riahi, K., Smith, S. J., Fujimori, S., Luderer, G., Kriegler, E., et al. (2019). Global emissions pathways under different socioeconomic scenarios for use in CMIP6: A dataset of harmonized emissions trajectories through the end of the century. *Geoscientific Model Development*, *12*(4), 1443–1475. https://doi.org/10.5194/gmd-12-1443-2019

Guenther, A., Karl, T., Harley, P., Wiedinmyer, C., Palmer, P. I., & Geron, C. (2006). Estimates of global terrestrial isoprene emissions using MEGAN (Model of Emissions of Gases and Aerosols from Nature). *Atmospheric Chemistry and Physics*, *6*, 3181–3210. https://doi.org/10.5194/acp-6-3181-2006

Heald, C. L., Ridley, D. A., Kroll, J. H., Barrett, S. R. H., Cady-Pereira, K. E., Alvarado, M. J., & Holmes, C. D. (2014). Contrasting the direct radiative effect and direct radiative forcing of aerosols. *Atmospheric Chemistry and Physics*, *14*(11), 5513–5527. https://doi.org/10.5194/acp-14-5513-2014

Hoesly, R. M., Smith, S. J., Feng, L. Y., Klimont, Z., Janssens-Maenhout, G., Pitkanen, T., et al. (2018). Historical (1750–2014) anthropogenic emissions of reactive gases and aerosols from the Community Emissions Data System (CEDS). *Geoscientific Model Development*, *11*(1), 369–408. https://doi.org/10.5194/gmd-11-369-2018

Huang, J., Pan, X., Guo, X., & Li, G. (2018). Health impact of China's Air Pollution Prevention and Control Action Plan: An analysis of national air quality monitoring and mortality data. *The Lancet. Planetary health*, *2*(7), e313–e323. https://doi.org/10.1016/s2542-5196(18)30141-4

Jacob, D. J. (2000). Heterogeneous chemistry and tropospheric ozone. *Atmospheric Environment*, *34*(12-14), 2131–2159. https://doi.org/10.1016/s1352-2310(99)00462-8

Jerrett, M., Burnett, R. T., Pope, C. A., Ito, K., Thurston, G., Krewski, D., et al. (2009). Long-term ozone exposure and mortality. *New England Journal of Medicine*, *360*(11), 1085–1095. https://doi.org/10.1056/NEJMoa0803894

Leibensperger, E. M., Mickley, L. J., Jacob, D. J., Chen, W. T., Seinfeld, J. H., Nenes, A., et al. (2012a). Climatic effects of 1950–2050 changes in US anthropogenic aerosols—Part 1: Aerosol trends and radiative forcing. *Atmospheric Chemistry and Physics*, *12*(7), 3333–3348. https://doi.org/10.5194/acp-12-3333-2012

Leibensperger, E. M., Mickley, L. J., Jacob, D. J., Chen, W. T., Seinfeld, J. H., Nenes, A., et al. (2012b). Climatic effects of 1950–2050 changes in US anthropogenic aerosols—Part 2: Climate response. *Atmospheric Chemistry and Physics*, *12*(7), 3349–3362. https://doi.org/10.5194/acp-12-3349-2012

Li, J. W., Han, Z. W., & Xie, Z. X. (2013). Model analysis of long-term trends of aerosol concentrations and direct radiative forcings over East Asia. *Tellus Series B: Chemical and Physical Meteorology*, *65*, 19. https://doi.org/10.3402/tellusb.v65i0.20410

Li, K., Jacob, D. J., Liao, H., Shen, L., Zhang, Q., & Bates, K. H. (2019). Anthropogenic drivers of 2013–2017 trends in summer surface ozone in China. *Proceedings of the National Academy of Sciences of the United States of America*, *116*, 422–427. https://doi.org/10.1073/pnas.1812168116

Li, K., Liao, H., Zhu, J., & Moch, J. M. (2016). Implications of RCP emissions on future PM2.5 air quality and direct radiative forcing over China. *Journal of Geophysical Research: Atmospheres*, *121*, 12985–13008. https://doi.org/10.1002/2016jd025623

Liu, H. Y., Jacob, D. J., Bey, I., & Yantosca, R. M. (2001). Constraints from Pb-210 and Be-7 on wet deposition and transport in a global three-dimensional chemical tracer model driven by assimilated meteorological fields. *Journal of Geophysical Research*, *106*(D11), 12109–12128. https://doi.org/10.1029/2000jd900839

Lu, X., Hong, J. Y., Zhang, L., Cooper, O. R., Schultz, M. G., Xu, X. B., et al. (2018). Severe surface ozone pollution in China: A global perspective. *Environmental Science & Technology Letters*, *5*(8), 487–494. https://doi.org/10.1021/acs.estlett.8b00366

Lu, X. C., Lin, C. Q., Li, W. K., Chen, Y., Huang, Y. Q., Fung, J. C. H., & Lau, A. K. H. (2019). Analysis of the adverse health effects of PM2.5 from 2001 to 2017 in China and the role of urbanization in aggravating the health burden. *Science of the Total Environment*, *652*, 683–695 . https://doi.org/10.1016/j.scitotenv.2018.10.140

Ma, Z. Q., Xu, J., Quan, W. J., Zhang, Z. Y., Lin, W. L., & Xu, X. B. (2016). Significant increase of surface ozone at a rural site, north of eastern China. *Atmospheric Chemistry and Physics*, *16*(6), 3969–3977. https://doi.org/10.5194/acp-16-3969-2016

McLinden, C. A., Olsen, S. C., Hannegan, B., Wild, O., Prather, M. J., & Sundet, J. (2000). Stratospheric ozone in 3-D models: A simple chemistry and the cross-tropopause flux. *Journal of Geophysical Research-Atmospheres*, *105*(D11), 14653–14665. https://doi.org/10.1029/2000jd900124

Park, R. J., Jacob, D. J., Chin, M., & Martin, R. V. (2003). Sources of carbonaceous aerosols over the United States and implications for natural visibility. *Journal of Geophysical Research-Atmospheres*, *108*(D12), 19. https://doi.org/10.1029/2002jd003190

Park, R. J., Jacob, D. J., Field, B. D., Yantosca, R. M., & Chin, M. (2004). Natural and transboundary pollution influences on sulfate-nitrate-ammonium aerosols in the United States: Implications for policy. *Journal of Geophysical Research-Atmospheres*, *109*(D15), 20. https://doi.org/10.1029/2003jd004473

Pozzoli, L., Janssens-Maenhout, G., Diehl, T., Bey, I., Schultz, M. G., Feichter, J., et al. (2011). Re-analysis of tropospheric sulfate aerosol and ozone for the period 1980-2005 using the aerosol-chemistry-climate model ECHAM5-HAMMOZ. *Atmospheric Chemistry and Physics*, *11*(18), 9563–9594. https://doi.org/10.5194/acp-11-9563-2011

Pye, H. O. T., Liao, H., Wu, S., Mickley, L. J., Jacob, D. J., Henze, D. K., & Seinfeld, J. H. (2009). Effect of changes in climate and emissions on future sulfate-nitrate-ammonium aerosol levels in the United States. *Journal of Geophysical Research*, *114*, D01205. https://doi.org/10.1029/2008jd010701

Qian, Y., Leung, L. R., Ghan, S. J., & Giorgi, F. (2003). Regional climate effects of aerosols over China: Modeling and observation. *Tellus Series B: Chemical and Physical Meteorology*, *55*(4), 914–934. https://doi.org/10.1046/j.1435-6935.2003.00070.x

Son, S. W., Tandon, N. F., Polvani, L. M., & Waugh, D. W. (2009). Ozone hole and Southern Hemisphere climate change. *Geophysical Research Letters*, *36*, L15705. https://doi.org/10.1029/2009gl038671

Sun, L., Xue, L. K., Wang, T., Gao, J., Ding, A. J., Cooper, O. R., et al. (2016). Significant increase of summertime ozone at Mount Tai in Central Eastern China. *Atmospheric Chemistry and Physics*, *16*(16), 10637–10650. https://doi.org/10.5194/acp-16-10637-2016

Thornton, J. A., Jaegle, L., & McNeill, V. F. (2008). Assessing known pathways for HO_2 loss in aqueous atmospheric aerosols: Regional and global impacts on tropospheric oxidants. *Journal of Geophysical Research-Atmospheres*, *113*(D5), 15. https://doi.org/10.1029/2007jd009236

Wang, W., Wu, J., Liu, H., Guo, S., Chen, X., & Luo, Y. (2005). Researches on the influence of pollution emission on tropospheric ozone variation and radiation over China and its adjacent area. *Chinese Journal of Atmospheric Sciences*, *29*(5), 734–746.

Wang, Y. H., Jacob, D. J., & Logan, J. A. (1998). Global simulation of tropospheric O-3-NOx-hydrocarbon chemistry 1. Model formulation. *Journal of Geophysical Research-Atmospheres*, *103*(D9), 10713–10725. https://doi.org/10.1029/98jd00158

van der Werf, G. R., Randerson, J. T., Giglio, L., van Leeuwen, T. T., Chen, Y., Rogers, B. M., et al. (2017). Global fire emissions estimates during 1997–2016. *Earth System Science Data*, *9*(2), 697–720. https://doi.org/10.5194/essd-9-697-2017

Wesely, M. L. (1989). Parameterization of surface resistances to gaseous dry deposition in regional-scale numerical-models. *Atmospheric Environment*, *23*(6), 1293–1304. https://doi.org/10.1016/0004-6981(89)90153-4

Xie, F., Li, J. P., Tian, W. S., Fu, Q., Jin, F. F., Hu, Y. Y., et al. (2016). A connection from Arctic stratospheric ozone to El Nino–Southern oscillation. *Environmental Research Letters*, *11*(12), 11. https://doi.org/10.1088/1748-9326/11/12/124026

Xie, F., Li, J. P., Zhang, J. K., Tian, W. S., Hu, Y. Y., Zhao, S., et al. (2017). Variations in North Pacific sea surface temperature caused by Arctic stratospheric ozone anomalies. *Environmental Research Letters*, *12*(11), 10. https://doi.org/10.1088/1748-9326/aa9005

Xie, F., Ma, X., Li, J. P., Huang, J. L., Tian, W. S., Zhang, J. K., et al. (2018). An advanced impact of Arctic stratospheric ozone changes on spring precipitation in China. *Climate Dynamics*, *51*(11-12), 4029–4041. https://doi.org/10.1007/s00382-018-4402-1

Zheng, B., Tong, D., Li, M., Liu, F., Hong, C. P., Geng, G. N., et al. (2018). Trends in China's anthropogenic emissions since 2010 as the consequence of clean air actions. *Atmospheric Chemistry and Physics*, *18*(19), 14095–14111. https://doi.org/10.5194/acp-18-14095-2018

Zhu, J., & Liao, H. (2016). Future ozone air quality and radiative forcing over China owing to future changes in emissions under the Representative Concentration Pathways (RCPs). *Journal of Geophysical Research: Atmospheres*, *121*, 1978–2001. https://doi.org/10.1002/2015jd023926

Ziemke, J. R., Oman, L. D., Strode, S. A., Douglass, A. R., Olsen, M. A., McPeters, R. D., et al. (2019). Trends in global tropospheric ozone inferred from a composite record of TOMS/OMI/MLS/OMPS satellite measurements and the MERRA-2 GMI simulation. *Atmospheric Chemistry and Physics*, *19*(5), 3257–3269. https://doi.org/10.5194/acp-19-3257-2019

References From the Supporting Information

Anenberg, S. C., Horowitz, L. W., Tong, D. Q., & West, J. J. (2010). An estimate of the global burden of anthropogenic ozone and fine particulate matter on premature human mortality using atmospheric modeling. *Environmental Health Perspectives*, *118*(9), 1189–1195. https://doi.org/10.1289/ehp.0901220

Huang, G. Y., Liu, X., Chance, K., Yang, K., Bhartia, P. K., Cai, Z. N., et al. (2017). Validation of 10-year SAO OMI Ozone Profile (PROFOZ) product using ozonesonde observations. *Atmospheric Measurement Techniques*, *10*(7), 21. https://doi.org/10.5194/amt-10-2455-2017

Ziemke, J. R., Chandra, S., Duncan, B. N., Froidevaux, L., Bhartia, P. K., Levelt, P. F., & Waters, J. W. (2006). Tropospheric ozone determined from aura OMI and MLS: Evaluation of measurements and comparison with the Global Modeling Initiative's Chemical Transport Model. *Journal of Geophysical Research-Atmospheres*, *111*(D19), 18. https://doi.org/10.1029/2006jd007089